Volume 14
Number 42
14 November 2023
Pages 11585–11926

Chemical Science

rsc.li/chemical-science

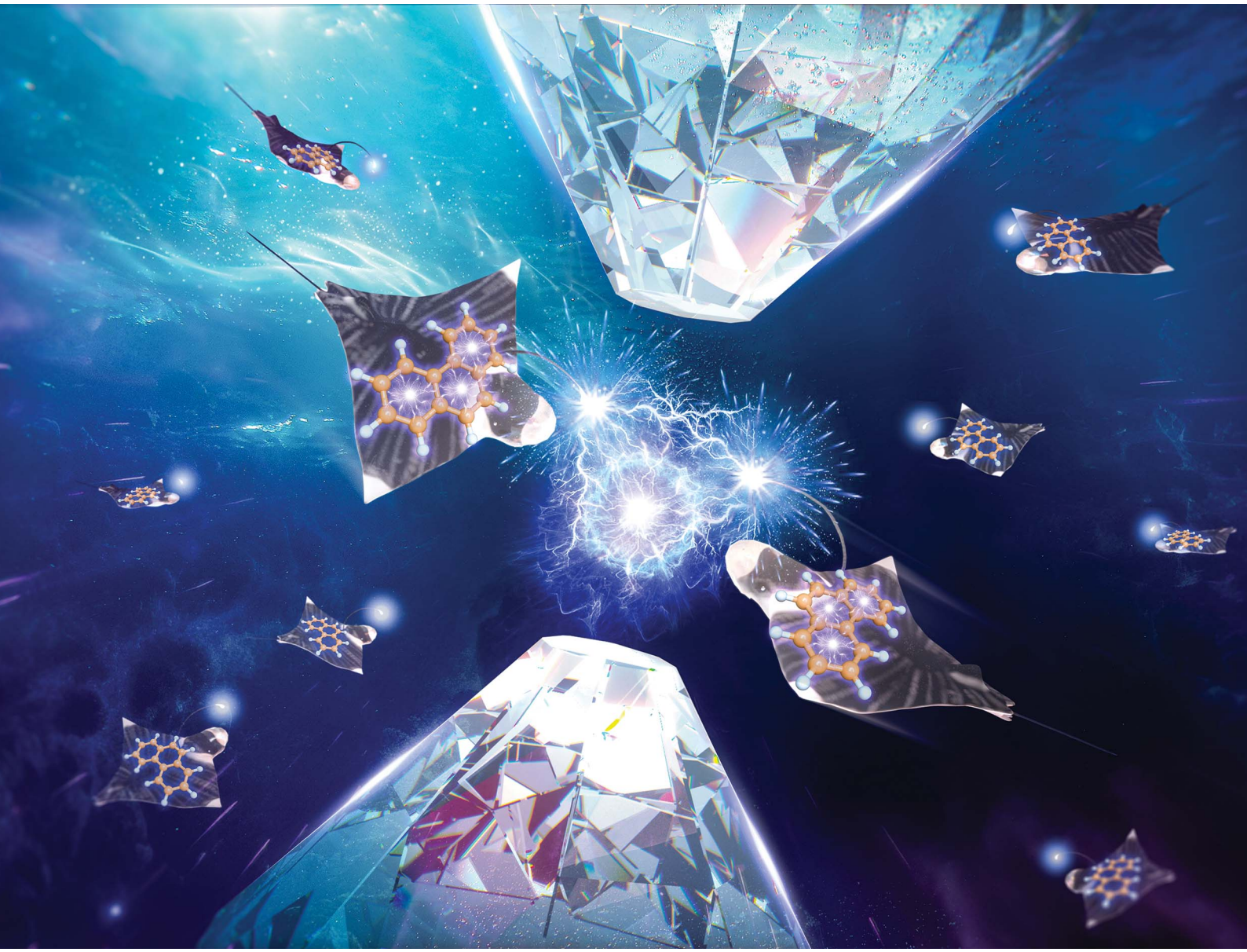

ISSN 2041-6539

ROYAL SOCIETY OF CHEMISTRY

EDGE ARTICLE

Chunguang Zhai, Mingguang Yao *et al.*

Realizing long range π-conjugation in phenanthrene and phenanthrene-based molecular crystals for anomalous piezoluminescence

Chemical Science

ROYAL SOCIETY OF CHEMISTRY

EDGE ARTICLE

View Article Online
View Journal | View Issue

Cite this: *Chem. Sci.*, 2023, **14**, 11629

All publication charges for this article have been paid for by the Royal Society of Chemistry

Received 1st August 2023
Accepted 2nd October 2023

DOI: 10.1039/d3sc04006b

rsc.li/chemical-science

Realizing long range π-conjugation in phenanthrene and phenanthrene-based molecular crystals for anomalous piezoluminescence†

Tongge Xu, Xiu Yin, Chunguang Zhai, * Desi Chen, Xiaoying Yang, Shuhe Hu, Kuo Hu, Yuchen Shang, Jiajun Dong, Zhen Yao, Quanjun Li, Peng Wang, Ran Liu, Mingguang Yao * and Bingbing Liu

Unlike the known aggregation-caused quenching (ACQ) that the enhancement of π–π interactions in rigid organic molecules usually decreases the luminescent emission, here we show that an intermolecular "head-to-head" π–π interaction in the phenanthrene crystal, forming the so-called "transannular effect", could result in a higher degree of electron delocalization and thus photoluminescent emission enhancement. Such a transannular effect is molecular configuration and stacking dependent, which is absent in the isomers of phenanthrene but can be realized again in the designed phenanthrene-based cocrystals. The transannular effect becomes more significant upon compression and causes anomalous piezoluminescent enhancement in the crystals. Our findings thus provide new insights into the effects of π–π interactions on luminescence emission and also offer new pathways for designing efficient aggregation-induced emission (AIE) materials to advance their applications.

Introduction

Solid-state luminescent materials have been attracting intensive research interest because of their wide range of applications, such as optoelectronics,[1–4] data storage[5,6] and theranostics.[7–9] Aggregation-induced emission (AIE) has been considered a dominant mechanism for designing organic solid luminescent materials for many applications.[10–19] In general, AIE molecules should be non-rigid with active intramolecular motions, and they usually show no emission in solutions at the molecular level but become brightly emissive in mesoscopic aggregated states.[20–22] For the AIE mechanism, it is generally accepted that the restriction of intramolecular motions (RIM) could reduce the energy dissipation channels of the non-radiative transition, enhance the radiative transition process and thus increase the emission in the aggregation state.[14,18]

Compared to non-rigid organic luminescent molecules, rigid organic molecules could exhibit additional advantages such as higher thermal stability and structural stability,[23,24] but rigid organic molecules usually show aggregation-caused quenching (ACQ)[13,14] in the aggregated state while becoming highly emissive in the isolated form.[25] In this case, the π–π stacking enhancement that should affect the π electron behaviors during excitation and radiation processes is considered as the main reason responsible for the ACQ.[26,27] Therefore, how to develop a new strategy to realize solid-state luminescent materials with high efficiency for new functionalities (such as piezoluminescence) and extended practical applications by using rigid organic molecules is highly desirable but remains challenging.

Numerous studies show that the delocalization and flowability of π electrons in organic luminescent molecules play important roles in their optical properties.[28–30] Graphene can be considered as an extremely large two-dimensional "conjugated molecule" constructed by substantial aromatic carbon rings,[31,32] in which π electrons exhibit high delocalization and also high flowability, leading to excellent electrical properties[33–35] but the absence of fluorescent properties. In contrast, when the number of aromatic rings decreases to the molecular level (such as polycyclic aromatic hydrocarbons, PAHs), π electrons tend to display heightened localization and reduced flowability because of the break of long range π-conjugation, which causes new properties and brings fluorescence emission.[36–38] Therefore, a possible way to design solid luminescent materials using rigid organic molecules is to promote the delocalization of π electrons without increasing their flowability, which remains a challenging task but is a new strategy different from those by decreasing π–π stacking. However, this has not been explored for the design of efficient luminescent materials.

High-pressure can be used to precisely tune intermolecular interactions, altering molecular vibration and rotation modes and electronic excited states, and thus manipulating the emission behaviors.[39–44] It is also an efficient technique to tune the delocalization of π electrons and amplify the related effects that

State Key Laboratory of Superhard Materials, College of Physics, Jilin University, Changchun 130012, China. E-mail: zhaicg@jlu.edu.cn; yaomg@jlu.edu.cn

† Electronic supplementary information (ESI) available. See DOI: https://doi.org/10.1039/d3sc04006b

are weak at ambient pressure. In this study, we discovered that the "transannular effect",[45–47] a type of weak π–π interaction, occurs in phenanthrene molecular crystals because of their unique molecular configuration. Such an effect becomes more significant upon compression and causes anomalous piezoluminescent enhancement in molecular crystals, which was also observed in phenanthrene-based cocrystals but absent in their isomers. The transannular effect could facilitate delocalization by generating long range π-conjugation in phenanthrene crystals while the flowability of π electrons is still limited within a single molecule, leading to an increase in radiative transition rates and emission intensity. Our finding not only adds another mechanism for aggregation-induced emission enhancement in luminescent materials but also presents an efficient strategy for the design of novel piezoluminescent materials.

Results and discussion

Experimental and theoretical details are presented in the ESI,† and structural information for all crystals and cocrystals involved in this work is presented in Fig. S1.† Fig. 1(a) displays the high-pressure photoluminescence (PL) spectra of phenanthrene crystals obtained by 360 nm excitation. The phenanthrene crystal shows split emission bands, similar to those of single molecules, which agrees well with the weak π–π stacking due to the bent geometry and a "herringbone" pattern[48] molecular arrangement in the phenanthrene crystal at ambient pressure (Fig. 1(f)). As shown in Fig. 1(b), phenanthrene shows anomalous emission enhancement at 1 atm–1.65 GPa as pressure increases, while at above 1.65 GPa, the emission exhibits the ACQ phenomenon (Fig. S2†). The quenched emission is primarily attributed to the compression-induced strengthening of intermolecular interactions, which results in more electron internal conversion and less radiation. *In situ* ultraviolet-visible (UV-vis) absorption spectra demonstrate that the energy gap was narrowed upon compression (Fig. 1(d and e)), leading to the red shift of emission.

The pressure-dependent PL intensities of phenanthrene crystals upon compression are shown in Fig. 1(c), revealing a significant intensity enhancement of about 5-fold up to 1.65 GPa. To elucidate the underlying reasons for such an anomalous emission enhancement, *in situ* infrared (IR) and Raman spectra measurements were performed to investigate the intra- and intermolecular interactions in the phenanthrene crystal under high pressure. The experimental results match the calculated results well (Fig. S3(c) and (d)†), and as shown in Fig. 2(a) and S4,† all IR absorption peaks are blue-shifted upon compression, indicating an increase in the intramolecular vibrational energies of phenanthrene and an increase of non-radiative processes.

We noticed that the IR absorption intensity at approximately 793 cm^{-1}, which represents the carbon skeleton out-of-plane bending vibration of the phenanthrene molecule according to our calculation, increases with pressure. The corresponding intensities of the 793 cm^{-1} mode as a function of pressure are plotted and shown in Fig. 2(b). This vibration mode exhibits a high degree of symmetry, and its intensity enhancement upon compression indicates that the molecule's dipole moment changes. This change may be due to the increased electronic delocalization of the intermediate aromatic ring because of the non-linear molecular structure of phenanthrene. Our Raman measurements show that all Raman modes are blue-shifted

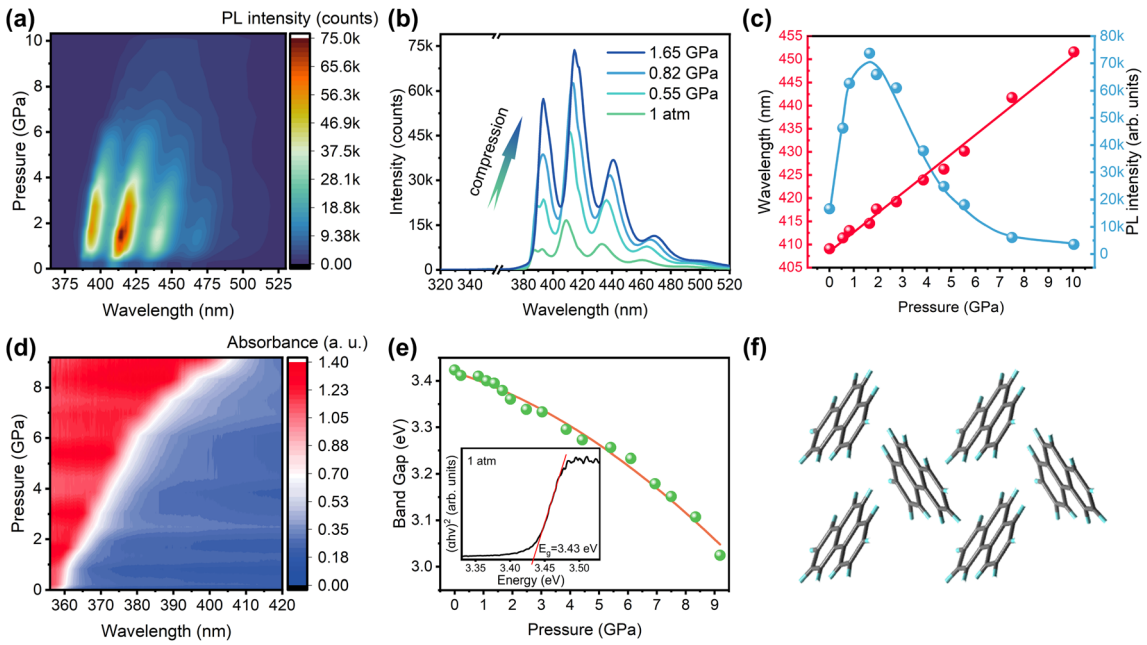

Fig. 1 (a) 2D colormap of pressure-dependent PL intensity and wavelength of the phenanthrene crystal. (b) *In situ* PL spectra of the phenanthrene crystal below 1.65 GPa. (c) Pressure-dependent PL wavelength and intensities. (d) 2D colormap of high-pressure UV-vis absorption spectra of the phenanthrene crystal. (e) Schematic illustrations of the band gap changes. (f) The sketch map for molecular packing of the phenanthrene crystal.

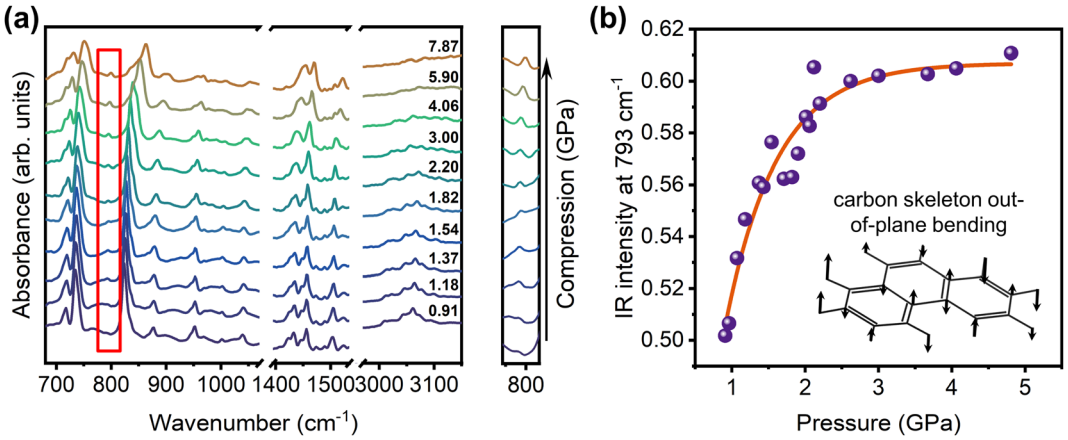

Fig. 2 (a) *In situ* IR spectra of the phenanthrene crystal upon compression. (b) The pressure-dependent IR absorption intensities around 793 cm^{-1} and the schematic diagram of the corresponding vibrational mode. The relevant vibrations are marked in the diagrams (a).

upon compression, which is consistent with our IR results (Fig. S3†). This clearly suggests that the general RIM mechanism cannot explain why phenanthrene exhibits such anomalous emission upon compression. Note that the Raman peaks around 100 cm^{-1} (see the marked regions in Fig. S3†) from out-of-plane carbon skeleton deformation vibrations exhibit a rapid blue shift at low pressure, implying significant interactions between the neighboring phenanthrene molecules, which may lead to a change in the π-electronic distribution on phenanthrene molecules. Combining our results from IR and Raman measurements, we suggest there is an active intermolecular nonbonding interaction – transannular effect. Note that previous studies show that the transannular effect can indeed alter the electronic structures of the aromatic system.[45,46,49,50] In our case, such a unique interaction that most likely occurs between phenanthrene molecules could lead to greater delocalization of π electrons, which can increase the radiative transition rates and result in an anomalous piezoluminescent enhancement.

To understand if the molecular stacking could favor the transannular effect in the crystal upon compression, a high-pressure X-ray diffraction (XRD) experiment has been carried

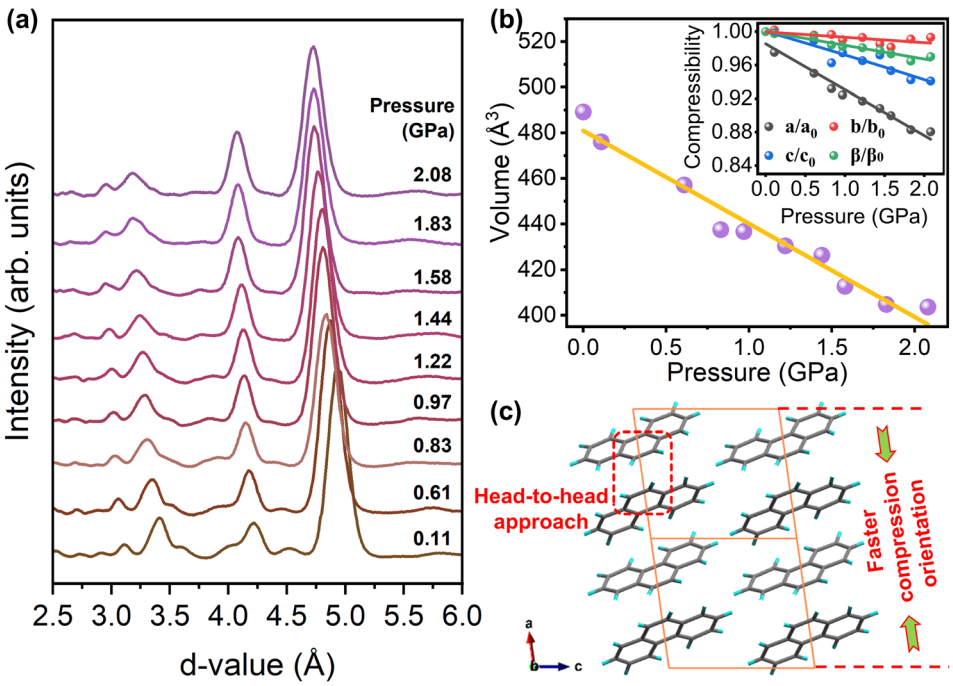

Fig. 3 (a) High-pressure XRD patterns of the phenanthrene crystal below 2.08 GPa. (b) Plotted curves for the unit cell volume of phenanthrene as a function of pressure. Inset shows the compression rate of lattice constants as pressure increases, which is given by the monoclinic $P2_1$ structure. (c) The crystal structure viewed along the *b*-axis, in which the marked regions represent the head-to-head approach between molecules. The XRD patterns are analyzed by JADE.

out on phenanthrene crystals. The recorded XRD patterns are presented in Fig. 3(a), wherein all the diffraction peaks are shifted to lower *d*-values, indicating compression of the lattice. Additionally, Fig. 3(b) depicts the variation of unit cell volume with pressure, showing that no structural transition occurred in the phenanthrene crystal during compression. Note that the *a*-, *b*-, and *c*-axes exhibit distinct pressure evolutions upon compression, implying an anisotropic compression of the lattice (inset, Fig. 3(b)). Furthermore, below 2.08 GPa, the *a*-axis was more compressible than the *b*- and *c*-axes, implying that the molecules become more closely packed along the *a*-axis, which is favorable for head-to-head π–π interactions between molecules (Fig. 3(c)). The Hirshfeld surface (HS) analysis[51–53] was performed to quantify and visualize the closed intermolecular atomic contacts in the phenanthrene crystal. The directions and strengths of intermolecular interactions within the molecular crystal are mapped onto the HS using the descriptor d_{norm}. The d_{norm} is essentially based on the two contact distances between the nearest atoms present inside (d_i) and outside (d_e) the surface, respectively, and is expressed as: $d_{norm} = (d_i - r_i^{vdw}/r_i^{vdw})/(d_e - r_e^{vdw}/r_e^{vdw})$, where r_i^{vdw} and r_e^{vdw} are the van der Waals radii of the appropriate atoms internal and external to the surface. The HS analysis also shows that high pressure can significantly enhance intermolecular interactions in head-to-head areas in phenanthrene crystals (Fig. S5†). Our structural analysis indicates that the aforementioned transannular delocalization effect is likely due to the close proximity of the head areas between phenanthrene molecules, which can lead to enhanced transannular effects. As shown in Fig. S5 (c and d),† the interactions between neighboring molecules were significantly enhanced, with an increase of 2.7% in C–H interactions from 1 atm to 2 GPa, respectively. Remarkably, the C–C interactions, which can be considered a π–π stacking interaction, increased by only 0.4% in the same pressure range, indicating that the transannular effects were more dominant than the π–π stacking effects below 2 GPa.

As we know, Fuzzy bond order (FBO)[54,55] was proposed to quantitatively describe the number of electron pairs shared between the fragments and has been used for the characterization of π-conjugation. Here FBO was thus calculated to analyze the conjugation of the head areas between neighboring phenanthrene molecules as shown in Fig. 3(c). The FBO is 0.19995 and 0.25464 for 1 atm and 2 GPa, respectively, indicating the increase of the transannular effect between neighboring phenanthrene molecules as pressure increases. On the other hand, the transannular effects should change the aromaticity of the molecules, and Harmonic oscillator measure of aromaticity (HOMA)[56] is the most popular geometry-based index for measuring aromaticity. HOMA was thus calculated and is shown in Table 1. The variation of HOMA was characterized by the three geometric segments of the phenanthrene molecule, which all show an increase in HOMA as pressure increases from 1 atm to 2 GPa. Note that the intermediate phenyl ring at the head (HOMA-2) exhibits the most significant increase from 0.476 to 0.551, indicating that the "head-to-head" interaction remarkably increases the delocalization of π-electrons on this aromatic ring. Such interactions can be considered as medium/long range π-conjugation, which is different from intermolecular π–π stacking. The theoretical calculations show that the proximity of adjacent phenanthrene molecules makes the transannular effect strengthened, which enhances the π-electron conjugation effect.

To obtain a further understanding of how the transannular effect caused the emission enhancement upon compression, we calculated the excited state properties of the phenanthrene crystal.[57] It is well known that the emission intensity of a system is proportional to the oscillator strength. We observed that the oscillator strength of emission in the phenanthrene crystal increases by an order of magnitude under high pressure as compared to that at ambient pressure (Fig. 4(a and b)), which agrees well with the observed emission enhancement in the experiment. The hole–electron analysis[58] was further performed to analyze the excitation characteristic of $S_1 \rightarrow S_0$. As shown in Fig. S6,† the photo-induced $S_1 \rightarrow S_0$ transition presents a locally excited (LE) feature at both ambient pressure and 2 GPa. Furthermore, the overlap function between hole and electron distribution can be defined as $S_r(r) = \sqrt{\rho^{hole}(r)\rho^{ele}(r)}$, in which ρ^{hole} and ρ^{ele} represent the densities of holes and electrons.[59] As shown in Fig. 4(c) and (d), the S_r is 0.75 and 0.82 for 1 atm and 2 GPa, respectively, indicating the increase of electron–hole overlap as pressure increases, which implies an increase in the orbital overlap between the excited state and ground state. This will increase the radiative transition probability and thus cause an enhancement of emission. In addition, it is found that the smaller the hole/electron delocalization index (HDI/EDI), the larger the spatial delocalization of the hole/electron.[59] The HDI and EDI of the phenanthrene crystal were calculated, which decrease from 1.92 to 1.67 and from 1.89 to 1.83, respectively, as pressure increases from 1 atm to 2 GPa, indicating an increase in spatial delocalization of the hole/electron upon compression. This is in agreement with the result obtained from the HOMA analysis. As shown in Fig. 4(e), the heat map of the hole, electron and hole–electron overlap for the three fragments is presented in Table 1, which shows that the intermediate aromatic ring plays a dominant role in the $S_1 \rightarrow S_0$ emission. Our theoretical simulations further demonstrate that head-to-head transannular delocalization alters the electronic structure of the phenanthrene molecule, which affects its emission.

The above results indicate that the transannular effect should be due to the bent geometry of phenanthrene. For

Table 1 The values of HOMA for each part of the phenanthrene molecule at 1 atm and 2 GPa

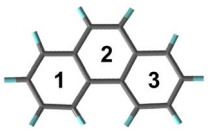

	HOMA-1	HOMA-2	HOMA-3
1 atm	0.840094	0.475597	0.844315
2 GPa	0.866979	0.550963	0.876380

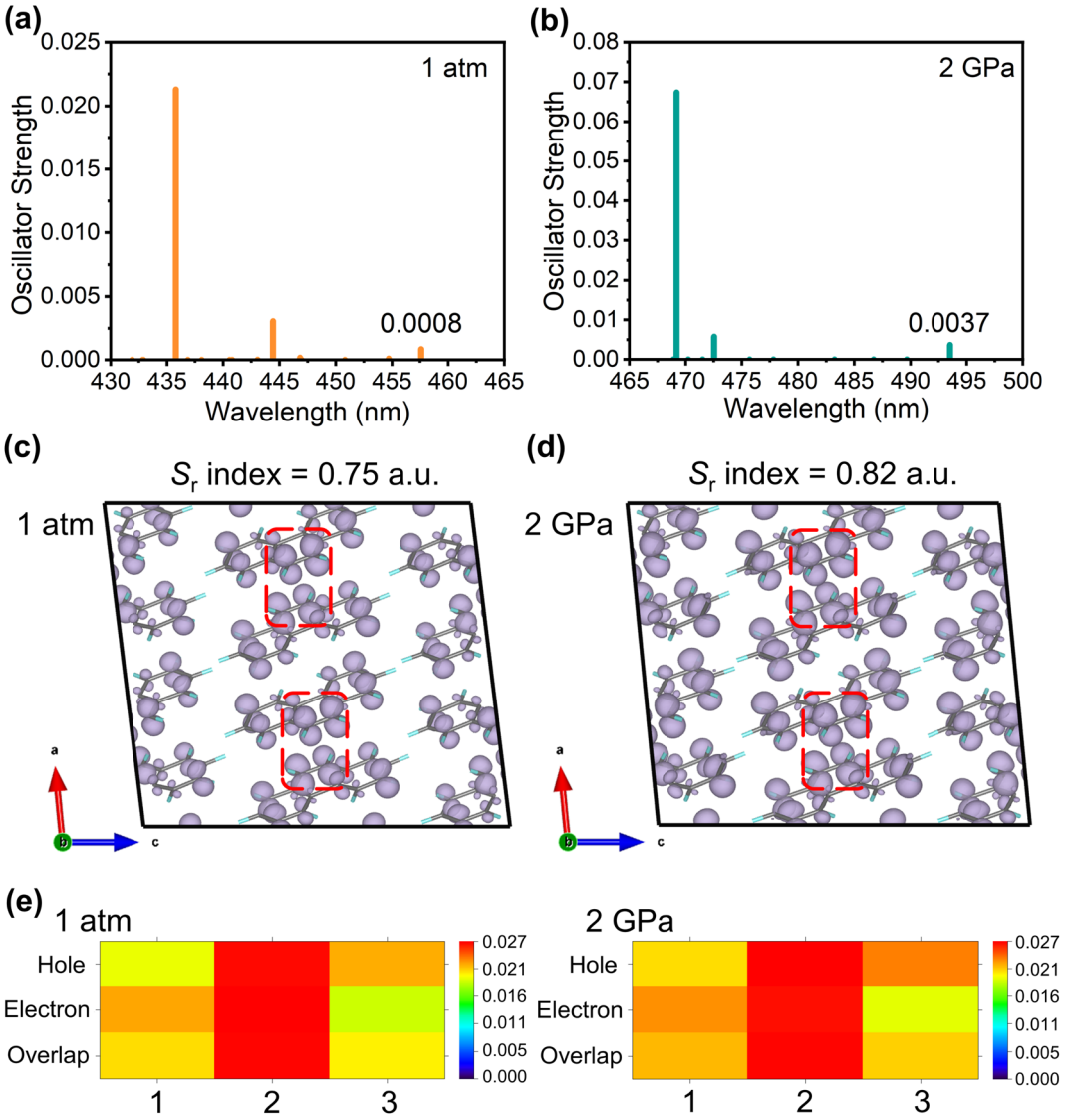

Fig. 4 (a and b) The emission oscillator strengths of phenanthrene calculated at 1 atm and 2 GPa. (c and d) The overlap function $S_r(r)$ during the $S_1 \rightarrow S_0$ transition at 1 atm and 2 GPa (isosurface level = 0.00016 a.u.), the marked regions represent the head-to-head areas between molecules. (e) The contributions of the three parts of the phenanthrene molecule (rings 1, 2, 3) to the hole, electron, and orbital overlap during the $S_1 \rightarrow S_0$ transition at 1 atm and 2 GPa.

comparison, the linear isomer of phenanthrene, anthracene, was studied and it exhibits a normal ACQ behavior accompanied by red-shifted emission upon compression in both experiments and calculations (Fig. S7(b–d)†), despite anthracene and phenanthrene having very similar molecular packing in the corresponding crystals (Fig. S7(a)†). The molecular configuration-dependent emission responses can be understood by the fact that the linear anthracene can easily form an excimer[60,61] and thus reduce the emission under high pressure, while the bent geometry is more favorable to suppress the increased π–π stacking between parallel phenanthrene molecules upon compression and provides a stronger steric effect. These differences in molecular configuration may be the reason why transannular effects do not occur in anthracene crystals.

We further demonstrate that the transannular effect could be either preserved or suppressed by introducing another component to form piezoluminescent cocrystals. Considering from molecular packing, we insert 1,2,4,5-tetracyanobenzene (TCNB) into phenanthrene (Phe) crystals, forming Phe–TCNB cocrystals. The TCNB could serve as an acceptor and hold the cocrystal's lowest unoccupied molecular orbital (LUMO), thereby simplifying the energy transfer route (charge-transfer (CT) emission). The TCNB could also prevent the face-to-face packing of phenanthrene molecules and thus leave only their head-to-head interactions (Fig. 5(a)). Our high-pressure PL spectra (Fig. 5(b)) reveal that the Phe–TCNB cocrystal indeed exhibits emission enhancement at a pressure range of 1 atm–1.77 GPa, but no structural phase change occurs in the cocrystals (Fig. S8†). The high-pressure IR absorption spectra of the Phe–TCNB cocrystal (Fig. S9†) also show that all IR absorption peaks were blue-shifted as pressure increased, indicating that the nonradiative energy dissipation of the molecule is not suppressed. Instead,

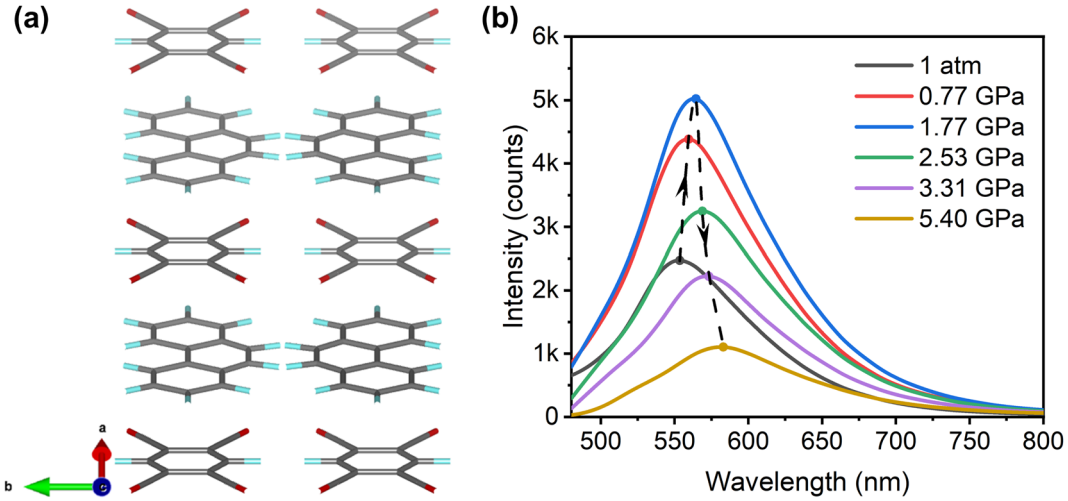

Fig. 5 (a) The sketch map for molecular packing of Phe–TCNB. (b) High-pressure PL spectra of Phe–TCNB.

the 796 cm^{-1} and 1602 cm^{-1} absorption peaks of Phe–TCNB from the carbon skeleton out-of-plane and in-plane bending display anomalous intensity enhancement as pressure increases, giving a strong indication for the transannular effect in this cocrystal. Note that when phenanthrene was replaced by its linear isomer anthracene (Ant), forming the Ant–TCNB cocrystal, emission quenching was observed upon compression (Fig. S10†). We could also destroy the head-to-head interactions between the phenanthrene molecules by inserting anthracene in Phe–TCNB cocrystals, forming a ternary $Ant_{0.5}$–$Phe_{0.5}$–TCNB cocrystal. In this case, the transannular effect was suppressed and emission quenching was observed upon compression (Fig. S11†). These results thus demonstrate that the transannular effect can be applicable to different luminescent materials, offering new pathways for designing more efficient organic luminescent materials for different applications.

Experimental and computational details

Materials source, synthesis and crystal structure

Phenanthrene (Phe, 98%) was purchased from Alfa Aesar, anthracene (Ant, 99%) was purchased from MACKLIN, and 1,2,4,5-tetracyanobenzene (TCNB, 97%) was purchased from Tokyo Chemical Industry Co., Ltd (TCI). All of the chemicals were used as received without further purification. The Phe–TCNB, Ant–TCNB and $Ant_{0.5}$–$Phe_{0.5}$–TCNB cocrystals were prepared by solvent evaporation methods. Identical molar masses of phenanthrene and TCNB were dissolved in excess tetrahydrofuran (THF) solutions and ultrasonicated for 12 minutes. The yellow stick-like transparent sample Phe–TCNB was obtained after evaporation of solvent from the solution after 3–4 days under ambient conditions. Ant–TCNB and $Ant_{0.5}$–$Phe_{0.5}$–TCNB cocrystals can be obtained by the same method. The initial crystal structures of our phenanthrene and anthracene were obtained from the Cambridge Crystallographic Data Centre (CCDC, no. 1232373 and no. 950158).

In situ high-pressure experiments

High-pressure experiments were performed in a diamond anvil cell (DAC). Samples were loaded into a 120 μm diameter hole drilled in the T301 stainless-steel gasket. Pressure was calibrated by the fluorescence emission of ruby in the sample chamber.[62] The pressure transmitting medium (PTM) used in the high-pressure PL, XRD, Raman and UV-vis absorption measurements was silicone oil, while it was KBr in the high-pressure IR measurements. A home-built integrated optical measurement system was used to collect high-pressure PL spectra and ultraviolet-visible (UV-vis) absorption spectra of phenanthrene and anthracene, and a semiconductor UV laser and a deuterium-halogen lamp were used as the excitation sources for the PL and absorption spectra, respectively, along with a Horiba Jobin Yvon iHR320 spectrometer; the PL excitation laser had a wavelength of 360 nm. And PL measurements of Phe–TCNB, Ant–TCNB and $Ant_{0.5}$–$Phe_{0.5}$–TCNB were performed on a Raman spectrometer equipped with a CCD detector (Renishaw in Via) in fluorescence mode, and a 514 nm line of a Cobolt FandangoTM laser was used for the excitation source. Infrared measurements were carried out using a Bruker Vertex 80 V spectrometer with a liquid nitrogen-cooled MCT detector. *In situ* high-pressure X-ray diffraction measurements were performed using a Rigaku Synergy Custom FR-X (λ = 0.7093 Å), while ambient-pressure X-ray diffraction measurements were performed using a Rigaku MicroMax-007 HF (λ = 1.5418 Å). High-pressure Raman spectra were collected using a LabRAM HR Evolution spectrometer (HORIBA Jobin-Yvon) excited by a 473 nm laser.

Computational details

The vibrational analysis was performed using the CASTEP[63] module in the Materials Studio package. The exchange and correlation of electrons were treated by the generalized gradient approximation (GGA) with the Perdew–Burke–Ernzerhof (PBE) functional, and the OTFG norm-conserving pseudo-potentials were used for calculations. We used the CP2K software

package[57] to perform geometry optimization and electronic structure simulation of a 2 × 2 × 2 supercell with 384 atoms. Our calculations employed the TZVP basis set, Goedecker–Teter–Hutter (GTH) pseudo-potential, PBE functional and dispersion corrected density functional (DFT-D3(BJ)), with a grid cutoff of 400 Ry. The relaxation of atomic positions and calculation of the electronic structure properties of excited states are performed by using linear response TDDFT for the singlet excited state. The CP2K input files, Fuzzy bond order (FBO) analysis,[54] hole–electron analysis[58] and HOMA analysis[56] were generated using the Multiwfn program.[55] The CrystalExplorer software 21.5 was employed to create Hirshfeld surface plots.[51–53] The lattice parameters at 1 atm and 2 GPa were calculated using the CP2K code by optimizing the energy of the geometry.

Conclusion

Our experiments and calculations strongly suggest that a unique transannular effect occurs in the phenanthrene crystal, which is related to its bent molecular geometry but absent in its isomers. The unique molecular geometry causes a typical head-to-head π–π interaction between phenanthrene molecules which can be modified by pressure, resulting in a higher degree of electron delocalization and thus an anomalous emission enhancement upon compression. Moreover, from the molecular stacking point of view, we succeeded in the design of phenanthrene-based cocrystals with the transannular effect and did observe similar piezoluminescence enhancement below 1.77 GPa. This indicates that the transannular effect can be active in both locally excited (LE) phenanthrene and charge-transfer (CT) phenanthrene-based cocrystals. Our findings contribute to a better understanding of the role of some typical π–π interactions on luminescence emission in highly aggregated conjugated systems and also provide a new way to design new organic AIE materials that could be used in stimulus response, optoelectronic devices, biomedical engineering, and other fields.

Data availability

Essential data are provided in the main text and the ESI.† Data can be available from the corresponding author upon reasonable request.

Author contributions

M. Y. and C. Z. conceived and supervised the study. T. X., C. Z. and D. C. designed and performed the experiments. C. Z., X. Y. and Z. Y. carried out the theoretical study. X. Y. carried out the structure analysis. S. H., K. H., Y. S., J. D., Q. L., P. W., R. L. and B. L. participated in the scientific discussions. T. X., M. Y. and C. Z. wrote and revised the manuscript.

Conflicts of interest

There are no conflicts to declare.

Acknowledgements

This work was supported financially by the National Natural Science Foundation of China (52225203, U2032215, 12304017, and 12104175), and the China Postdoctoral Science Foundation (2022M720054). We thank the Shanghai Synchrotron Radiation Facility and Beijing Synchrotron Radiation Facility. We also thank the Instrument and Equipment Sharing Platform, College of Physics, Jilin University for the XRD measurements.

References

1 A. Setaro, M. Adeli, M. Glaeske, D. Przyrembel, T. Bisswanger, G. Gordeev, F. Maschietto, A. Faghani, B. Paulus and M. Weinelt, Preserving π-conjugation in covalently functionalized carbon nanotubes for optoelectronic applications, *Nat. Commun.*, 2017, **8**, 14281.
2 Y. Han, L. Bai, J. Lin, X. Ding, L. Xie and W. Huang, Diarylfluorene-Based Organic Semiconductor Materials toward Optoelectronic Applications, *Adv. Funct. Mater.*, 2021, **31**, 2105092.
3 A. C. Grimsdale, K. Leok Chan, R. E. Martin, P. G. Jokisz and A. B. Holmes, Synthesis of light-emitting conjugated polymers for applications in electroluminescent devices, *Chem. Rev.*, 2009, **109**, 897–1091.
4 G. M. Farinola and R. Ragni, Electroluminescent materials for white organic light emitting diodes, *Chem. Soc. Rev.*, 2011, **40**, 3467–3482.
5 M. Irie, T. Fukaminato, T. Sasaki, N. Tamai and T. Kawai, A digital fluorescent molecular photoswitch, *Nature*, 2002, **420**, 759–760.
6 M. Irie, T. Fukaminato, K. Matsuda and S. Kobatake, Photochromism of diarylethene molecules and crystals: memories, switches, and actuators, *Chem. Rev.*, 2014, **114**, 12174–12277.
7 K. Li and B. Liu, Polymer-encapsulated organic nanoparticles for fluorescence and photoacoustic imaging, *Chem. Soc. Rev.*, 2014, **43**, 6570–6597.
8 G. Feng and B. Liu, Aggregation-induced emission (AIE) dots: emerging theranostic nanolights, *Acc. Chem. Res.*, 2018, **51**, 1404–1414.
9 Y. Huang, X. You, L. Wang, G. Zhang, S. Gui, Y. Jin, R. Zhao and D. Zhang, Pyridinium-substituted tetraphenylethylenes functionalized with alkyl chains as autophagy modulators for cancer therapy, *Angew. Chem., Int. Ed.*, 2020, **132**, 10128–10137.
10 H. Zhang, Z. Zhao, A. T. Turley, L. Wang, P. R. McGonigal, Y. Tu, Y. Li, Z. Wang, R. T. Kwok and J. W. Lam, Aggregate science: from structures to properties, *Adv. Mater.*, 2020, **32**, 2001457.
11 F. Würthner, Aggregation-induced emission (AIE): a historical perspective, *Angew. Chem., Int. Ed.*, 2020, **59**, 14192–14196.
12 S. Suzuki, S. Sasaki, A. S. Sairi, R. Iwai, B. Z. Tang and G. i. Konishi, Principles of aggregation-induced emission: design of deactivation pathways for advanced AIEgens and applications, *Angew. Chem., Int. Ed.*, 2020, **59**, 9856–9867.

13 J. Mei, N. L. Leung, R. T. Kwok, J. W. Lam and B. Z. Tang, Aggregation-induced emission: together we shine, united we soar, *Chem. Rev.*, 2015, **115**, 11718–11940.
14 J. Mei, Y. Hong, J. W. Lam, A. Qin, Y. Tang and B. Z. Tang, Aggregation-induced emission: the whole is more brilliant than the parts, *Adv. Mater.*, 2014, **26**, 5429–5479.
15 Q. Li and Z. Li, The strong light-emission materials in the aggregated state: what happens from a single molecule to the collective group, *Adv. Sci.*, 2017, **4**, 1600484.
16 F. Hu, S. Xu and B. Liu, Photosensitizers with aggregation-induced emission: materials and biomedical applications, *Adv. Mater.*, 2018, **30**, 1801350.
17 Y. Hong, J. W. Lam and B. Z. Tang, Aggregation-induced emission, *Chem. Soc. Rev.*, 2011, **40**, 5361–5388.
18 Y. Hong, J. W. Lam and B. Z. Tang, Aggregation-induced emission: phenomenon, mechanism and applications, *Chem. Commun.*, 2009, 4332–4353.
19 X. Cai and B. Liu, Aggregation-induced emission: recent advances in materials and biomedical applications, *Angew. Chem., Int. Ed.*, 2020, **59**, 9868–9886.
20 J. Luo, Z. Xie, J. W. Lam, L. Cheng, H. Chen, C. Qiu, H. S. Kwok, X. Zhan, Y. Liu and D. Zhu, Aggregation-induced emission of 1-methyl-1,2,3,4,5-pentaphenylsilole, *Chem. Commun.*, 2001, 1740–1741.
21 B. Z. Tang, Photoluminescence and electroluminescence of hexaphenylsilole are enhanced by pressurization in the solid state, *Chem. Commun.*, 2008, 2989–2991.
22 H. T. Feng, Y. X. Yuan, J. B. Xiong, Y. S. Zheng and B. Z. Tang, Macrocycles and cages based on tetraphenylethylene with aggregation-induced emission effect, *Chem. Soc. Rev.*, 2018, **47**, 7452–7476.
23 S. E. Stein and R. Brown, π-Electron properties of large condensed polyaromatic hydrocarbons, *J. Am. Chem. Soc.*, 1987, **109**, 3721–3729.
24 J. D. Dunitz and A. Gavezzotti, Attractions and repulsions in molecular crystals: what can be learned from the crystal structures of condensed ring aromatic hydrocarbons?, *Acc. Chem. Res.*, 1999, **32**, 677–684.
25 J. B. Birks, *Photophysics of Aromatic Molecules*, 1970.
26 Y. Huang, J. Xing, Q. Gong, L. C. Chen, G. Liu, C. Yao, Z. Wang, H. L. Zhang, Z. Chen and Q. Zhang, Reducing aggregation caused quenching effect through co-assembly of PAH chromophores and molecular barriers, *Nat. Commun.*, 2019, **10**, 169.
27 M. Park, Y. Jeong, H. S. Kim, W. Lee, S. H. Nam, S. Lee, H. Yoon, J. Kim, S. Yoo and S. Jeon, Quenching-Resistant Solid-State Photoluminescence of Graphene Quantum Dots: Reduction of π–π Stacking by Surface Functionalization with POSS, PEG, and HDA, *Adv. Funct. Mater.*, 2021, **31**, 2102741.
28 W. Zhu, R. Zheng, Y. Zhen, Z. Yu, H. Dong, H. Fu, Q. Shi and W. Hu, Rational design of charge-transfer interactions in halogen-bonded co-crystals toward versatile solid-state optoelectronics, *J. Am. Chem. Soc.*, 2015, **137**, 11038–11046.
29 Y. C. Wei, K. H. Kuo, Y. Chi and P. T. Chou, Efficient Near-Infrared Luminescence of Self-Assembled Platinum (II) Complexes: From Fundamentals to Applications, *Acc. Chem. Res.*, 2023, **56**, 689–699.
30 Y. Liu, S. Jiang, K. Glusac, D. H. Powell, D. F. Anderson and K. S. Schanze, Photophysics of monodisperse platinum-acetylide oligomers: delocalization in the singlet and triplet excited states, *J. Am. Chem. Soc.*, 2002, **124**, 12412–12413.
31 X. Y. Wang, X. Yao and K. Müllen, Polycyclic aromatic hydrocarbons in the graphene era, *Sci. China: Chem.*, 2019, **62**, 1099–1144.
32 R. Gutzler and D. F. Perepichka, π-Electron conjugation in two dimensions, *J. Am. Chem. Soc.*, 2013, **135**, 16585–16594.
33 Y. W. Choi and H. J. Choi, Dichotomy of electron-phonon coupling in graphene moire flat bands, *Phys. Rev. Lett.*, 2021, **127**, 167001.
34 Y. Cao, V. Fatemi, S. Fang, K. Watanabe, T. Taniguchi, E. Kaxiras and P. Jarillo-Herrero, Unconventional superconductivity in magic-angle graphene superlattices, *Nature*, 2018, **556**, 43–50.
35 K. I. Bolotin, F. Ghahari, M. D. Shulman, H. L. Stormer and P. Kim, Observation of the fractional quantum Hall effect in graphene, *Nature*, 2009, **462**, 196–199.
36 Y. Yamaguchi, Y. Matsubara, T. Ochi, T. Wakamiya and Z. Yoshida, How the π conjugation length affects the fluorescence emission efficiency, *J. Am. Chem. Soc.*, 2008, **130**, 13867–13869.
37 K. P. Loh, Q. Bao, G. Eda and M. Chhowalla, Graphene oxide as a chemically tunable platform for optical applications, *Nat. Chem.*, 2010, **2**, 1015–1024.
38 L. Cao, M. J. Meziani, S. Sahu and Y. P. Sun, Photoluminescence properties of graphene versus other carbon nanomaterials, *Acc. Chem. Res.*, 2013, **46**, 171–180.
39 C. Zhai, X. Yin, S. Niu, M. Yao, S. Hu, J. Dong, Y. Shang, Z. Wang, Q. Li and B. Sundqvist, Molecular insertion regulates the donor–acceptor interactions in cocrystals for the design of piezochromic luminescent materials, *Nat. Commun.*, 2021, **12**, 4084.
40 X. Yin, C. Zhai, S. Hu, L. Yue, T. Xu, Z. Yao, Q. Li, R. Liu, M. Yao and B. Sundqvist, Doping of charge-transfer molecules in cocrystals for the design of materials with novel piezo-activated luminescence, *Chem. Sci.*, 2023, **14**, 1479–1484.
41 H. Liu, Y. Gu, Y. Dai, K. Wang, S. Zhang, G. Chen, B. Zou and B. Yang, Pressure-induced blue-shifted and enhanced emission: a cooperative effect between aggregation-induced emission and energy-transfer suppression, *J. Am. Chem. Soc.*, 2020, **142**, 1153–1158.
42 Y. Dong, B. Xu, J. Zhang, X. Tan, L. Wang, J. Chen, H. Lv, S. Wen, B. Li and L. Ye, Piezochromic luminescence based on the molecular aggregation of 9, 10-Bis ((E)-2-(pyrid-2-yl) vinyl) anthracene, *Angew. Chem., Int. Ed.*, 2012, **51**, 10782–10785.
43 T. Zhang, X. Yong, J. Yu, Y. Wang, M. Wu, Q. Yang, X. Hou, Z. Liu, K. Wang and X. Yang, Brightening Blue Photoluminescence in Nonemission MOF-2 by Pressure Treatment Engineering, *Adv. Mater.*, 2023, **35**, 2211729.

44 J. Fang, Z. Fu, X. Chen, Y. Liu, F. Chen, Y. Wang, H. Li, Y. Yusran, K. Wang and V. Valtchev, Piezochromism in Dynamic Three-Dimensional Covalent Organic Frameworks, *Angew. Chem., Int. Ed.*, 2023, e202304234.

45 W. Wang, J. Xu and Y. H. Lai, Alternating Conjugated and Transannular Chromophores: Tunable Property of Fluorene-Paracyclophane Copolymers via Transannular π–π Interaction, *Org. Lett.*, 2003, **5**, 2765–2768.

46 D. J. Cram and R. H. Bauer, Macro Rings. XX. Transannular Effects in π–π-Complexes1, *J. Am. Chem. Soc.*, 1959, **81**, 5971–5977.

47 M. E. Stoll, S. R. Lovelace, W. E. Geiger, H. Schimanke, I. Hyla-Kryspin and R. Gleiter, Transannular Effects in Dicobalta–Superphane Complexes on the Mixed-Valence Class II/Class III Interface: Distinguishing between Spin and Charge Delocalization by Electrochemistry, Spectroscopy, and ab Initio Calculations, *J. Am. Chem. Soc.*, 1999, **121**, 9343–9351.

48 J. Dhar, D. P. Karothu and S. Patil, Herringbone to cofacial solid state packing via H-bonding in diketopyrrolopyrrole (DPP) based molecular crystals: influence on charge transport, *Chem. Commun.*, 2015, **51**, 97–100.

49 X. Pang, H. Wang, X. R. Zhao and W. J. Jin, Co-crystallization turned on the phosphorescence of phenanthrene by C–Br⋯π halogen bonding, π–hole⋯π bonding and other assisting interactions, *CrystEngComm*, 2013, **15**, 2722–2730.

50 H. Y. Gao, X. R. Zhao, H. Wang, X. Pang and W. J. Jin, Phosphorescent cocrystals assembled by 1, 4-diiodotetrafluorobenzene and fluorene and its heterocyclic analogues based on C–I⋯π halogen bonding, *Cryst. Growth Des.*, 2012, **12**, 4377–4387.

51 J. Bojarska, M. Remko, A. Fruziński and W. Maniukiewicz, The experimental and theoretical landscape of a new antiplatelet drug ticagrelor: Insight into supramolecular architecture directed by CH⋯F, π⋯π and CH⋯π interactions, *J. Mol. Struct.*, 2018, **1154**, 290–300.

52 M. A. Spackman and J. J. McKinnon, Fingerprinting intermolecular interactions in molecular crystals, *CrystEngComm*, 2002, **4**, 378–392.

53 M. A. Spackman and D. Jayatilaka, Hirshfeld surface analysis, *CrystEngComm*, 2009, **11**, 19–32.

54 I. Mayer and P. Salvador, Overlap populations, bond orders and valences for 'fuzzy'atoms, *Chem. Phys. Lett.*, 2004, **383**, 368–375.

55 T. Lu and F. Chen, Multiwfn: A multifunctional wavefunction analyzer, *J. Comput. Chem.*, 2012, **33**, 580–592.

56 T. M. Krygowski, Crystallographic studies of inter-and intramolecular interactions reflected in aromatic character of. pi.-electron systems, *J. Chem. Inf. Comput. Sci.*, 1993, **33**, 70–78.

57 T. D. Kühne, M. Iannuzzi, M. Del Ben, V. V. Rybkin, P. Seewald, F. Stein, T. Laino, R. Z. Khaliullin, O. Schütt and F. Schiffmann, CP2K: An electronic structure and molecular dynamics software package-Quickstep: Efficient and accurate electronic structure calculations, *J. Chem. Phys.*, 2020, **152**, 194103.

58 Z. Liu, T. Lu and Q. Chen, An sp-hybridized all-carboatomic ring, cyclo [18] carbon: Bonding character, electron delocalization, and aromaticity, *Carbon*, 2020, **165**, 468–475.

59 Y. Shao, T. Lu, M. Li and W. Lu, Theoretical exploration of diverse electron-deficient core and terminal groups in A–DA′ D–A type non-fullerene acceptors for organic solar cells, *New J. Chem.*, 2022, **46**, 3370–3382.

60 P. F. Jones and M. Nicol, Excimer fluorescence of crystalline anthracene and naphthalene produced by high pressure, *J. Chem. Phys.*, 1965, **43**, 3759–3760.

61 J. Birks, *Rep. Prog. Phys.*, 1975, **38**, 903.

62 H. Mao, J. A. Xu and P. Bell, Calibration of the ruby pressure gauge to 800 kbar under quasi-hydrostatic conditions, *J. Geophys. Res.: Solid Earth*, 1986, **91**, 4673–4676.

63 S. J. Clark, M. D. Segall, C. J. Pickard, P. J. Hasnip, M. I. Probert, K. Refson and M. C. Payne, First principles methods using CASTEP, *Z. Kristallogr. – Cryst. Mater.*, 2005, **220**, 567–570.